Ultramicroscopy 111 (2011) 285–289

Contents lists available at ScienceDirect

Ultramicroscopy

journal homepage: www.elsevier.com/locate/ultramic

Direct oxygen imaging within a ceramic interface, with some observations upon the dark contrast at the grain boundary

S.D. Findlay [a,*], S. Azuma [a], N. Shibata [a,b], E. Okunishi [c], Y. Ikuhara [a,d,e]

[a] Institute of Engineering Innovation, The University of Tokyo, Tokyo 116-0013, Japan
[b] PRESTO, Japan Science and Technology Agency, Saitama 332-0012, Japan
[c] JEOL Ltd., Tokyo 196-8558, Japan
[d] Nanostructures Research Laboratory, Japan Fine Ceramic Center, Nagoya 456-8587, Japan
[e] WPI Advanced Institute for Materials Research, Tohoku University, Sendai 980-8577, Japan

ARTICLE INFO

Article history:
Received 15 November 2010
Received in revised form
15 December 2010
Accepted 17 December 2010
Available online 28 December 2010

Keywords:
Scanning transmission electron microscopy (STEM)
High-angle annular dark field (HAADF)
Annular bright field (ABF)

ABSTRACT

Annular bright field scanning transmission electron microscopy, which has recently been established to produce directly interpretable images with both light and heavier atomic columns visible simultaneously, is shown to allow directly interpretable imaging of the oxygen columns within the Σ13 [1 $\bar{2}$ 1 0](1 0 $\bar{1}$ 4) pyramidal twin grain boundary in α−Al_2O_3. By using information in the high-angle annular dark field image and annular bright field images simultaneously, we estimate the specimen thickness and finite source size, and use them to explore in simulation the issue of dark contrast in the vicinity of the grain boundary in the annular dark field image.

1. Introduction

High-angle annular dark field scanning transmission electron microscopy (HAADF STEM) has been established as a direct and robust imaging mode for determining the location of heavy atom columns within grain boundaries [1,2]. However, light elements are usually not visible in HAADF STEM. Structural analysis using the observed positions of only the heavy elements as reference points to compare with candidate structure models, perhaps determined by molecular dynamics or first principles calculations, has had some success. For instance, simulations in an α−Al_2O_3 Σ13 grain boundary show an oxygen-terminated trial structure to be consistent with the experimental HAADF image while an aluminum-terminated structure is not, even though the oxygen itself was not imaged [3]. High voltage electron microscopy [4], negative C_s imaging conventional TEM [5] and exit surface wavefunction reconstruction [6] have all been used to image oxygen within grain boundaries and defect structures. However, these approaches are not yet routine, requiring very thin specimens and detailed simulation for interpretation and analysis [7]. By contrast, for bulk crystals, annular bright field (ABF) STEM imaging allows for direct image interpretation with both light and heavy atom columns simultaneously visible over a wide range of thicknesses [8–10]. In this paper we demonstrate that this property extends to the case of light atoms in a defect structure, specifically a grain boundary.

2. Experimental results

Our case study will be the pristine Σ13 (1 0 $\bar{1}$ 4) pyramidal twin grain boundary in α−Al_2O_3, which has been studied previously in high resolution TEM experiments [12,13], STEM experiments [3] and first principles calculations [3,11,14]. STEM imaging was carried out on the JEOL ARM-200F, operated at 200 keV with a probe-forming aperture semiangle of 22 mrad. HAADF images were taken with a 90–170 mrad detector, ABF images with a 11–22 mrad detector. Representative HAADF and ABF images based on these imaging conditions are shown in Fig. 1 for bulk α−Al_2O_3 [15]. The known structure is overlaid on the images. Inspection reveals that there are two types of oxygen column: those in close proximity to an adjacent aluminium column and those approximately equidistant from the aluminium–oxygen column pairs. In the HAADF image, the oxygen columns of the aluminium–oxygen column pairs are not resolved, though there is some directional elongation of the signal from the aluminium column of the pair. There is a hint of contrast visible at the isolated oxygen columns in the HAADF image, but it is not very clear. In the ABF image, however, oxygen columns are much more visible. The isolated oxygen columns are clearly resolved. The oxygen columns in the aluminium–oxygen column pairs are less clearly resolved, but are evident in the asymmetric contrast of the column

* Corresponding author. Tel.: +81 3 5841 7756; fax: +81 3 5841 7694.
E-mail address: scott@sigma.t.u-tokyo.ac.jp (S.D. Findlay).

0304-3991/$ - see front matter © 2010 Elsevier B.V. All rights reserved.
doi:10.1016/j.ultramic.2010.12.022

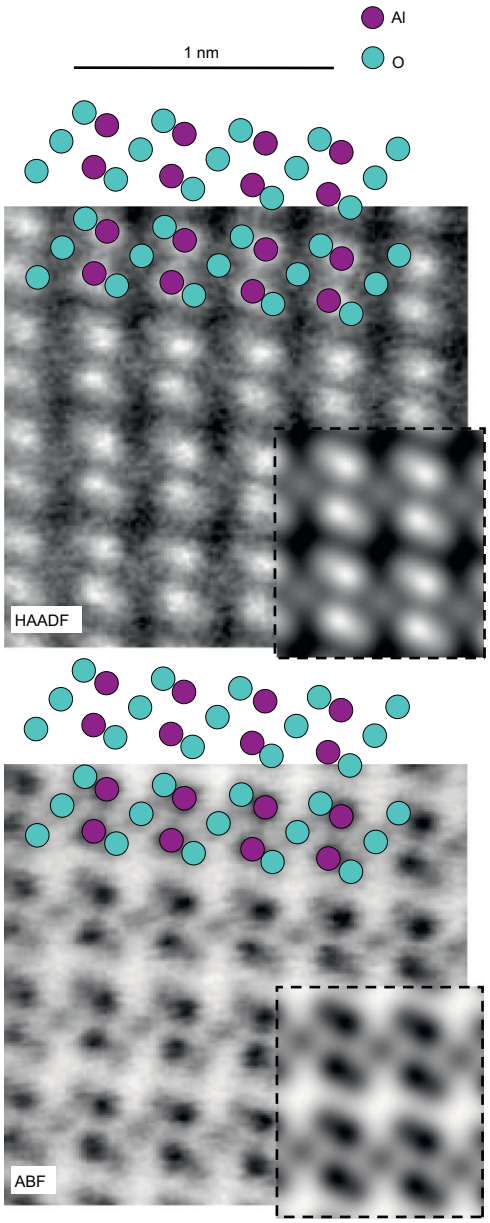

Fig. 1. HAADF and ABF images of α−Al_2O_3 (bulk) viewed along the [1 $\overline{2}$ 1 0] zone axis. The known structure is indicated, and simulated data is overlaid on the experimental images. The experimental images have been filtered using the radial difference filter released by HREM Research Inc [16].

pair to a much greater extent than was the case in the HAADF image. Simulated images are overlaid on the experimental images in Fig. 1. The simulations assume the experimental parameters listed above, a 381 Å specimen thickness and a finite effective source size of 0.37 Å. As discussed in Section 3, these values offer a particularly favourable comparison with these experimental images, but the robustness of the imaging mode is such that good qualitative agreement between simulation and experiment is obtainable even if the specimen thickness cannot readily be determined [10].

HAADF and ABF images of the grain boundary region are shown in Fig. 2. As seen in Fig. 1 for the bulk region, the oxygen columns are not visible in the HAADF image in Fig. 2. Similar to previous images of this grain boundary, the structure in the boundary region is obscured by the dark band of contrast [3]. In the ABF image, however, oxygen columns in the bulk and, moreover, in the grain boundary are visible. The structural model for the oxygen-terminated grain boundary determined by first principles calculations [3,11] is overlaid on both images. The agreement, particularly with the ABF image, is generally very good, though we note that in the enlarged portion of the ABF image the oxygen columns in the grain boundary appear to be slightly displaced to the left as compared with the symmetric structural model reference. There is also a suggestion that the troughs corresponding to the oxygen columns in the grain boundary in the experimental ABF image are slightly wider than those in the bulk, though against the scan noise in the image it is difficult to tell if this perception is statistically significant.

The dark region in the vicinity of the grain boundary, a common observation in such experiments, is not reproduced in the simulations based on the structure determined from first principles calculations. Reasons for this—such as that the first principles structure model does not include preferential milling, vacancies or the possibility of co-existence with meta-stable structure—have been suggested previously [3]. All these possibilities fall under the general area of defect structures, and indeed by standard definitions the grain boundary is a defect structure all by itself. The clarity of the ABF image, which shows only a very weak variation in the contrast in the vicinity of the grain boundary region, demonstrates that ABF is the more robust technique for identifying column locations within defect structure while HAADF is the more sensitive technique for indicating the presence of the defect itself, as was previously predicted in simulation [10].

3. Simulation results and the dark contrast at the grain boundary

One factor hindering attempts to understand the reduced contrast at grain boundaries is the difficulty of measuring elementary specimen parameters like thickness. Preferential milling in a highly localized region could be a plausible explanation if the specimen thickness was such that the change seen in the contrast represented the loss of only a couple of atomic layers, but not if it implies, say, 5 Å wide but 50 Å deep grooves in the specimen. In our experiment, ABF imaging was realized using a bright field detector and a beam stop, a geometry which precluded simultaneous recording of a low-loss spectrum which might otherwise have provided some information on specimen thickness and perhaps its possible variation near the interface. The robustness of HAADF imaging works against us in attempting to determine the thickness from the HAADF image alone, and the image contrast also depends significantly on the effective source size (spatial incoherence) [17], another parameter which is difficult to measure directly. The specimen thickness and finite source size cannot be determined simultaneously from a single experimental image, but here we have two: the HAADF and ABF images. We can therefore try to determine these two unknowns by matching to the contrast in both HAADF and ABF images simultaneously. (Contrary to earlier suggestions that STEM suffers from a contrast problem similar to that reported in conventional TEM [19], on the basis of recent work [18,20,21] we take it as given that comparison between the simulated and experimental contrast is both possible and meaningful.)

To this end, boxes ‘A’, ‘B’, ‘a’ and ‘b’, positioned away from the interface region to be more representative of the bulk material, are used to obtain the projected scans shown at the right in Fig. 2. Such projection avoids the worst effects of noise and image distortion, but reducing all the image detail to a single number is fairly crude: identical contrast need not imply identical images. The projected scans have sinusoidal appearance and least squares fitting to the form $ax+b+c\cos(dx+e)$ was applied. In this expression, ax is a linear term allowing for a slow variation across the image, b gives

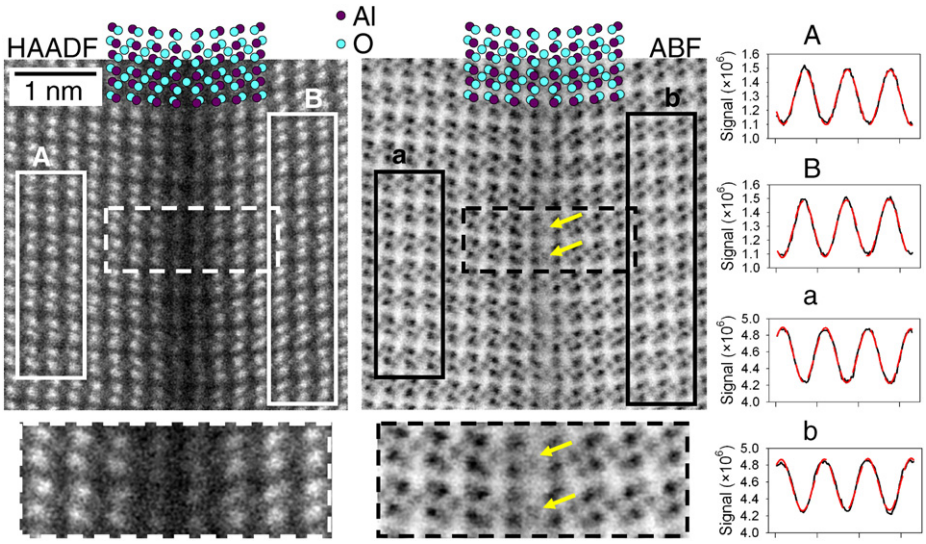

Fig. 2. Experimental HAADF and ABF images of the $\Sigma 13\,(1\,0\,\bar{1}\,4)$ grain boundary in α–Al_2O_3 viewed along the $[1\,\bar{2}\,1\,0]$ zone axis. The images were smoothed by a smoothing filter incorporated in DigitalMicrograph, Gatan. The area in the dashed rectangle is magnified below the images. The arrows indicate the location of two of the oxygen columns which are clearly visible in the grain boundary region. The first principles determined structure [3,11] is indicated. The plots at the right show the signal resulting from projection in the vertical direction of the regions in boxes marked 'A', 'B', 'a' and 'b'. The dashed lines show the least squares fit to the form $ax+b+c\cos(dx+e)$ (see the discussion in Section 3).

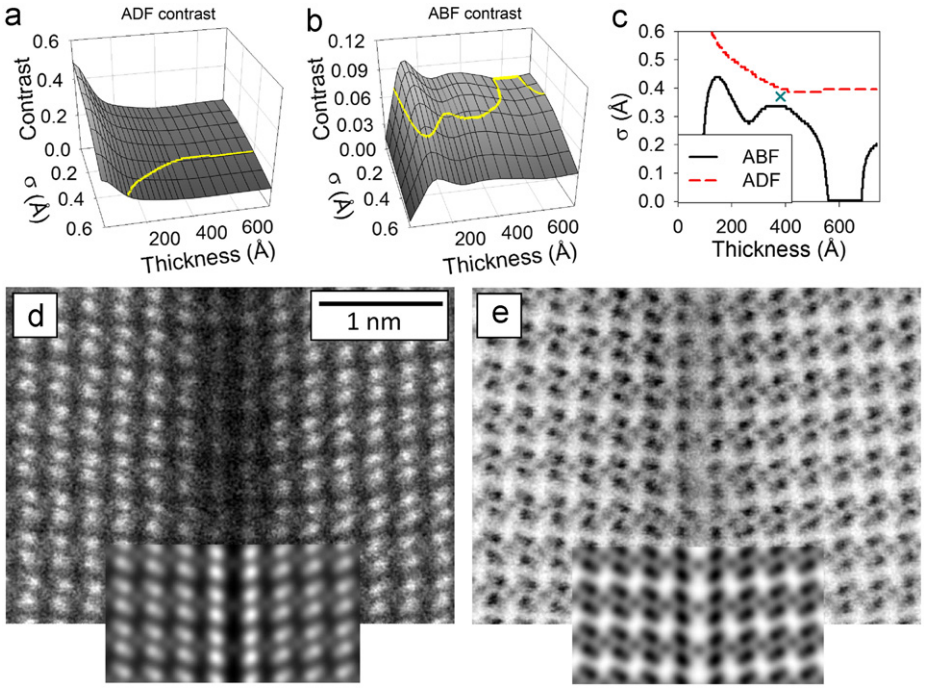

Fig. 3. Simulated contrast in projections over (a) HAADF and (b) ABF images as a function of specimen thickness and finite effective source size σ. The contour line shows the contrast determined from the plots in Fig. 2. (c) The thickness–σ dependence of the isocontours in agreement with the experimental data. The two plots on this graph do not intersect, but the cross indicates the point deemed to constitute the best agreement. (d) HAADF and (e) ABF experimental images, as per Fig. 2, with overlaid simulations for the thickness–σ combination indicated by the cross in (c).

the mean offset, and c gives the amplitude of the sinusoidal oscillation with spatial frequency d and lateral shift e. Including the linear term improves the fit, but the linear term is relatively small and we neglect it in taking the Michelson visibility—$(I_{max}-I_{min})/(I_{max}+I_{min})$—definition of contrast, giving c/b. This gives the following contrast values: A, 0.151; B, 0.159; a, 0.072; b, 0.067. The differences in values across the interface may indicate differences in tilt, but are quite small. HAADF and ABF images for the bulk material as a function of thickness and finite source size, σ, were simulated using the experimental parameters given above and including temporal incoherence assuming a chromatic aberration coefficient of $C_c=1.63$ mm and a full-width-half-maximum energy spread of 1 eV. For some thickness–σ combinations, projected scans of the simulated data display more structure than does the experimental data. Therefore, contrast was defined using the maximum and minimum values of the projected simulations directly, without fitting to a sinusoidal form. The resultant contrast surface plots are shown in Figs. 3(a) and (b), with the contour lines indicating the contrast from the experimental images (averaged across the two sides of the interface).

Fig. 3(c) shows the relation between thickness and σ which agrees with the experimental data. Given that contrast is a crude measure, we were not guaranteed to get a unique intercept, but in fact we get no intercept at all. The success of recent quantitative comparisons between STEM experiment and simulation gives us confidence that the simulations are not deficient in what they explicitly include [17,18]. There has been some suggestion that characterizing the parameters of aberration-corrected microscopes well enough to allow for these sorts of comparisons is more demanding than in the uncorrected case [22]. Moreover, not all imaginable effects are included in these simulations. The simulated HAADF images for the smaller thicknesses only match the experimental contrast for large values of σ, for which the resolution in the simulations is clearly lower than that in the experiments. This suggests the experimental HAADF contrast is lower than ideally expected, perhaps through mis-tilt or the presence of amorphous layers (a carbon layer coating had been deposited on the present sample).

Attempting to include additional, uncharacterized effects would put us back in the position of trying to constrain too many unknowns with too few images. Instead, let us take a good compromise thickness $-\sigma$ combination, 381 and 0.37 Å respectively, as indicated by the cross in Fig. 3(c). Figs. 3(d) and (e) are overlaid with simulations for these parameters and using the first principles determined oxygen-terminated interface structure model. Away from the interface these simulations are in good agreement with the experiment, though close inspection suggests the distinguishability of columns in the adjacent aluminium–oxygen pairs in the ABF image may be slightly greater in the experimental data than in the simulation. One might also, on the basis of Fig. 3(c), have considered the thickness–σ combination of 191 and 0.47 Å as a good compromise. However, while this gives a

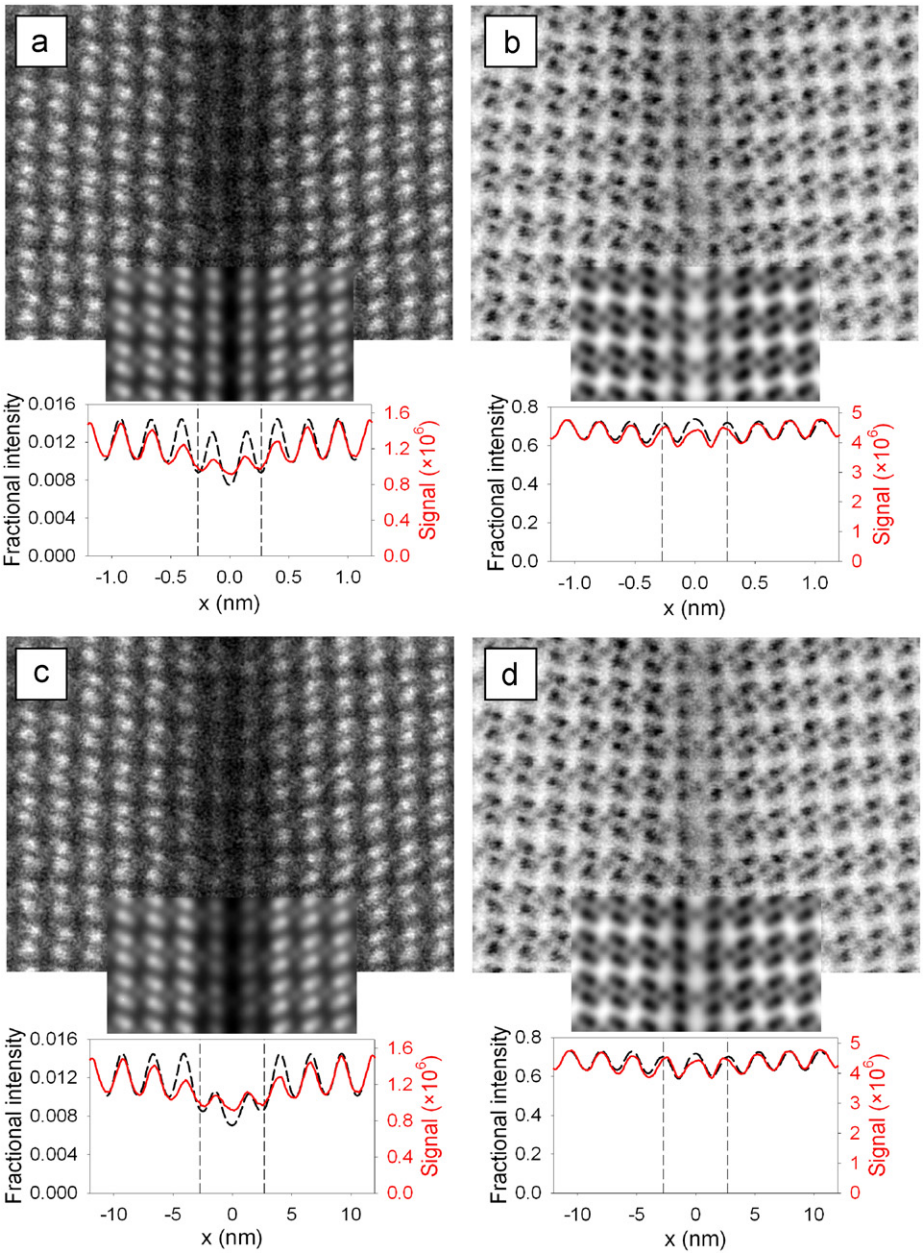

Fig. 4. (a) HAADF and (b) ABF experimental images with overlaid simulations for a specimen modelling preferential milling by removing 38 Å of material from both the top and bottom surfaces at the grain boundary. (c) HAADF and (d) ABF experimental images with overlaid simulations for artificially distorted columns in the vicinity of the grain boundary. The region of modified material is indicated by the dashed vertical lines on the plots. All simulations use the thickness–σ combination determined in Fig. 3.

similarly good match by the single measure of contrast, the larger source size produces an image in which the resolution is notably poorer than the experiment, and we discard this parameter combination on those grounds.

The contrast in the vicinity of the grain boundary in the HAADF image differs notably between experiment and simulation. As found previously [3], relaxations near the grain boundary in the first principles structural model are not enough to account for the dark contrast. In fact, the aluminium–oxygen column pair nearest the boundary is brighter in the simulation than those further away. This can be understood from the structural model. The relaxed structure reduces the spacing between these columns near the grain boundary, and the increased intensity in the simulation is a simple consequence of the greater overlap of these two columns. The simulations assume the Debye–Waller factor for aluminium and oxygen atoms in the grain boundary is the same as for those in bulk. This is probably not true, but the simulations are insensitive to modest variations in these values.

Let us take the agreement in the images away from the boundary as being encouraging that our thickness–σ estimate is reasonable. Using these values we can ask what degree of preferential milling would be required to produce the change in contrast seen in the experimental image. Figs. 4(a) and (b) again show extracts from the experimental HAADF and ABF images, and the overlaid simulations are based on a structure which crudely mocks up preferential milling by removing 38 Å of material from both the top and bottom surfaces in the vicinity of the grain boundary. Line scans projected along the direction of the interface are shown below each figure. It seems that there is little effect on the ABF image, while the intensity in the HAADF image is reduced. However, while the average intensity reduces by about the necessary amount, this is a reduction in the "background" signal. The height of the column pair signal above the background has not been significantly altered, in contradiction to the experimental data. So the images seem inconsistent, and anyway removing 38 Å of material from an area of about 10 Å width via ion milling without chemical etching is a little hard to believe. It does not rule out such milling as a partial contributor, but suggests against it being the entire explanation. That simulations even with this milling overestimate the local column contrast suggests that the columns are more distorted and/or vacancy-ridden than our idealized model suggests. Without providing a specific physical justification, but following from previous explorations in simulation [10], let us assess the effect of introducing random static displacements into the columns in the vicinity of the grain boundary. We apply a random lateral displacement to each atom along the column independently by an amount such that the displacements follow a normal distribution with a 0.3 Å standard deviation. The result is shown in Figs. 4(c) and (d).

The appearance of this simulation is more in keeping with the experimental data. We have confined the displacements to the layers nearest the boundary, though the experiment suggests that the effect extends out to the second and third layers with decreasing magnitude. It must be admitted that displacements with a standard deviation of 0.3 Å are larger than can realistically be anticipated by strain alone. However, it has been shown that vacancies have a very similar effect in HAADF and ABF images to that of such random displacements [10], and the presence of vacancies would additionally produce significant local distortions. That vacancy formation is easier in the $\Sigma 13$ α–Al_2O_3 grain boundary than in the bulk has already been demonstrated [23].

4. Conclusion

In summary, two points are particularly significant. First, being able to see the location of light element columns in the grain boundary is important for detailed analysis and gives us increased confidence in the first principles calculated structure. Second, ABF is more robust than HAADF for imaging column locations within defect structures, whereas the HAADF intensity is more sensitive than that of ABF to the presence of the defect structures. The current technique does not, as some previous analyses do [4–6], enable us to quantitatively assess an oxygen vacancy distribution at the boundary. But it does enable a direct identification of the presence and location of the oxygen columns in the grain boundary, without the need for simulations, largely irrespective of the specimen thickness. It would be too much to say that we have conclusively established the cause for the dark contrast in the grain boundary region of the HAADF image, but the evidence here strongly supports vacancy-induced strain as the dominant mechanism. Regardless, ABF has been seen to be less sensitive to defects than HAADF and therefore is the more robust technique for determining column locations in the vicinity of the grain boundary. Having a simultaneously recorded ABF image gives both a clearer picture of the grain boundary structure and also an additional handle to pin down some other quantities which affect the interpretation of contrast but are often difficult to measure directly.

Acknowledgements

This work was supported in part by the Grant-in-Aid for Scientific Research on Priority Areas "Nano Materials Science for Atomic-scale Modification 474" from the Ministry of Education, Culture, Sports and Technology (MEXT) of Japan. N.S. acknowledges supports from PRESTO, Japan Science and Technology Agency, and from New Energy and Industrial Technology Development Organization (NEDO).

References

[1] G. Duscher, M.F. Chisholm, U. Alber, M. Rühle, Nat. Mater. 3 (2004) 621.
[2] J.P. Buban, K. Matsunaga, J. Chen, N. Shibata, W.Y. Ching, T. Yamamoto, Y. Ikuhara, Science 311 (2006) 212.
[3] S. Azuma, N. Shibata, S.D. Findlay, T. Mizoguchi, T. Yamamoto, Y. Ikuhara, Philos. Mag. Lett. 90 (2010) 539.
[4] Z. Zhang, W. Sigle, F. Phillipp, M. Rühle, Science 302 (2003) 846.
[5] C.L. Jia, K. Urban, Science 303 (2004) 2001.
[6] C.L. Jia, A. Thust, K. Urban, Phys. Rev. Lett. 95 (2005) 225506.
[7] K. Urban, Nat. Mater. 8 (2009) 260.
[8] E. Okunishi, I. Ishikawa, H. Sawada, F. Hosokawa, M. Hori, Y. Kondo, Microsc. Microanal. 15 (Suppl. 2) (2009) 164.
[9] S.D. Findlay, N. Shibata, H. Sawada, E. Okunishi, Y. Kondo, T. Yamamoto, Y. Ikuhara, Appl. Phys. Lett. 95 (2010) 191913.
[10] S.D. Findlay, N. Shibata, H. Sawada, E. Okunishi, Y. Kondo, Y. Ikuhara, Ultramicroscopy 110 (2010) 903.
[11] K. Nakamura, T. Mizoguchi, N. Shibata, K. Matsunaga, T. Yamamoto, Y. Ikuhara, Phys. Rev. B 75 (2007) 184109.
[12] T. Höche, P.R. Kenway, H.-J. Kleebe, M.W. Finnis, M. Rühle, J. Phys. Chem. Solids 55 (1994) 1067.
[13] T. Höche, M. Rühle, J. Am. Ceram. Soc. 79 (1996) 1961.
[14] S. Fabris, C. Elsässer, Phys. Rev. B 64 (2001) 245117.
[15] These images are actually cropped from images which include the grain boundary. However, at a few layers removed from the boundary plane no evidence of structure or contrast variation due to the interface remains in the images, and as such they are considered to be reasonably representative of bulk material.
[16] 〈http://www.hremresearch.com/〉.
[17] J.M. LeBeau, S.D. Findlay, L.J. Allen, S. Stemmer, Phys. Rev. Lett. 100 (2008) 206101.
[18] J.M. LeBeau, A.J. D'Alfonso, S.D. Findlay, S. Stemmer, L.J. Allen, Phys. Rev. B 80 (2009) 174106.
[19] D.O. Klenov, S. Stemmer, Ultramicroscopy 106 (2006) 889.
[20] J.M. LeBeau, S.D. Findlay, X. Wang, A.J. Jacobson, L.J. Allen, S. Stemmer, Phys. Rev. B 79 (2009) 214110.
[21] J.M. LeBeau, A.J. D'Alfonso, S.D. Findlay, L.J. Allen, S. Stemmer, Phys. Rev. B 80 (2009) 174106.
[22] Y. Kotaka, Ultramicroscopy 110 (2010) 555.
[23] N. Takahashi, T. Mizoguchi, T. Tohei, K. Nakamura, T. Nakagawa, N. Shibata, T. Yamamoto, Y. Ikuhara, Mater. Trans. 50 (2009) 1019.